Undersea Biomedical Research, Vol. 13, No. 1, March 1986

In vivo microbubble detection in decompression sickness using a second harmonic resonant bubble detector

C. L. CHRISTMAN, P. W. CATRON, E. T. FLYNN, and P. K. WEATHERSBY

U.S. Department of Health and Human Services, Food and Drug Administration, Center for Devices and Radiological Health, 5600 Fishers Lane, Rockville, MD 20857; and Hyperbaric Medicine Program Center, Naval Medical Research Institute, Naval Medical Command National Capital Region, Bethesda, MD 20814

Christman CL, Catron PW, Flynn ET, Weathersby PK. In vivo microbubble detection in decompression sickness using a second harmonic resonant bubble detector. Undersea Biomed Res 1986; 13(1):1–18.—A resonant bubble detection method based on a second harmonic technique has been used to monitor the femoral vascular system of dogs subjected to rapid decompression. For this study, the detector consisted of two acoustic transducers mounted at right angles to each other that were packaged in a perivascular cuff configuration. This detector responds selectively only to bubbles near resonant size (4.2 μm in diameter); solid particles and large bubbles produce no response. The detector was used to monitor a total of 15 dogs. Eleven dogs were subjected to a series of simulated underwater dives until acute symptoms of decompression sickness occurred; 4 dogs served as controls. In the dived group, either the femoral vein or the femoral artery was monitored. Resonant bubbles were observed in the femoral veins of all 6 dogs monitored at this location. During arterial monitoring, most dogs showed no response, but an occasional weak response was observed in 2 of the dogs. No resonant bubbles were detected in the femoral artery or the femoral vein in any of the controls. The data suggest that this bubble detection method is feasible for in vivo use. Furthermore, 4 μm diameter bubbles are much more prevalent in the veins of dogs suffering from decompression sickness than they are in dog arteries, presumably because they are filtered out effectively by the pulmonary circulation. Modifications of this method are discussed to enhance its accuracy and applicability for quantifying bubble size, location, and number.

microbubble detection
decompression sickness
ultrasonic bubble detection
resonance
nonlinear
second harmonic
implanted probe

In vivo bubble detection is important in a variety of different fields, including surgery (1), extracorporeal oxygenation monitoring (2), and decompression procedures (3). Ultrasonic detection methods have traditionally been used because they offer advantages as both nontraumatic and noninvasive techniques. Although numer-

ous ultrasonic methods have been developed over the past 15 yr, no single method yet fulfills all the requirements of an ideal detector, which should identify only microbubbles and indicate their size, location, and number.

The most commonly used ultrasonic device for bubble detection is the Doppler flowmeter (4–6). It offers many advantages for the detection of intravascular bubbles, including good sensitivity, ease of use, and the availability of inexpensive commercial equipment. Unfortunately, Doppler devices respond not only to bubbles but also to movement of red blood cells, pulsating vessel walls, valve and other heart sounds, and occasional motion of the probe. A more fundamental problem with Doppler devices is that they detect only moving bubbles. B mode pulse-echo imaging systems have been modified to detect both moving and stationary bubbles in a wide range of different tissues (7, 8). The latter systems have the additional advantage of determining bubble location and size, although for bubbles with diameters smaller than 300 μm, a complex relationship exists between bubble size and image size (9).

The advantages of using a resonance technique to detect bubbles are well documented (10–12). Because bubbles resonate, but red cell masses, thrombi, platelet aggregates, and lipid emboli do not, this method differentiates between bubbles and solid or liquid particles. The production of discrete bursts of ultrasound allows detection of bubble location relative to the transducer. The resonance technique also allows identification of stationary as well as moving bubbles, and offers advantages in signal detection. The main problem associated with resonance techniques involves the separation of resonant signals from reflected signals.

Recently, Miller (13) developed a probe suitable for in vivo use that takes a novel approach to the above problem. It is based on the principle that for incident field amplitudes of sufficient magnitude, a bubble's oscillation is nonlinear. Thus, by detecting the second harmonic emission, the probe filters out reflected signals and responds only to resonant signals. Miller's prototype device operates in a continuous wave (CW) mode at a fixed frequency and is packaged in a perivascular cuff configuration. Therefore it responds to only one size bubble, does not indicate the bubble's position, and can only be used for vascular measurements. In theory, the device could be modified to operate over a range of frequencies to detect different bubble sizes, to transmit in pulsed mode to localize the bubbles' positions relative to the transducer, and to be packaged to monitor stationary as well as moving bubbles in a variety of different tissues. Although the device had been tested extensively in vitro, no in vivo measurements have yet been obtained. The purpose of this study was to demonstrate and evaluate the operation of the resonant bubble detector (RBD) in vivo. For this purpose the vascular systems of dogs subjected to rapid decompression were monitored with the RBD.

THEORY

If a bubble is placed in an acoustic field where the ultrasonic wavelength is long compared to the radius of the bubble, pressure variations within the incident field will cause the radius of the bubble to oscillate. As a consequence, acoustic energy is scattered or reradiated from the bubble. In this study, this reradiated energy served as a means of bubble detection. As the magnitude of the acoustic field increases, the

bubble oscillations become nonlinear for resonant-size bubbles, creating an appreciable second harmonic component, even for incident fields of moderate intensity.

By using truncated polynomial expansions, Miller (13) was able to obtain a solution to a nonlinear equation of motion for pulsating bubbles that provides a method to calculate the scattered pressure amplitudes of both the first and second harmonics. As Miller's calculations assume a bubble pulsating in water, they may not apply to bubbles in blood. In an attempt to investigate bubble differences expected for blood, we used Miller's formulation to calculate both the first and second harmonic amplitudes for a bubble in water, plasma, and whole blood. The equations needed for these calculations are included in the Appendix, and Table 1 lists the physical parameters used, where gamma is the ratio of the specific heat at constant pressure in air to the specific heat at constant volume in air.

The calculations also depend on the bubble's total damping coefficient and its stiffness. The damping coefficient is the sum of three components: radiation, thermal, and viscous damping. Each component was evaluated using equations provided by Nishi (14), which are identical to an earlier formulation (17), except for the thermal damping term that has been modified to account for the bubble's surface tension. The bubble's stiffness, also computed from an equation provided by Nishi, is used to calculate the polytropic exponent (18). The results of calculations for scattered pressure amplitude are shown in Fig. 1 for plasma and whole blood; the results for water are not included because they virtually overlap the curve for plasma.

Figure 1 illustrates some of the advantages of the second harmonic emission detection method. The output from most other acoustic detection methods, including Doppler and pulse-echo visualization, is provided by the scattered amplitude curve of the first harmonic. For these devices, the largest bubble produces the greatest response. In contrast, the resonant bubble detector, RBD, whose output is provided by the scattered amplitude curve of the second harmonic, responds selectively. Only bubbles near resonant size (4.2 μm in diameter at 1.62 MHz for an air bubble in water) will produce a response. The maximum response occurs for bubbles at resonant size, but decreases by a factor of 10 with a change in radius of only 25%. In addition, only bubbles are likely to convert a significant portion of the incident field into a second harmonic signal. Thus, in contrast to the output from a Doppler device, moving red blood cells will not produce a response when the RBD is used. Also in

TABLE 1

PHYSICAL PROPERTIES OF WATER, WHOLE BLOOD, AND BLOOD PLASMA USED TO CALCULATE SCATTERED PRESSURE AMPLITUDE (6, 14–16)

	Water 20°C	Blood 37°C	Plasma 37°C
Density ($Kg \cdot m^{-3}$)	988	1056	1025
Velocity ($m \cdot s^{-1}$)	1481	1570	1548
Surface Tension ($N \cdot m^{-1}$)	0.072	0.060	0.050
Viscosity ($N \cdot s \cdot m^{-2}$)	0.001	0.00303	0.0013
Thermal Diffusivity ($m^2 \cdot s^{-1}$)	2.7×10^{-5}	2.7×10^{-5}	2.7×10^{-5}
Gamma	1.4	1.4	1.4

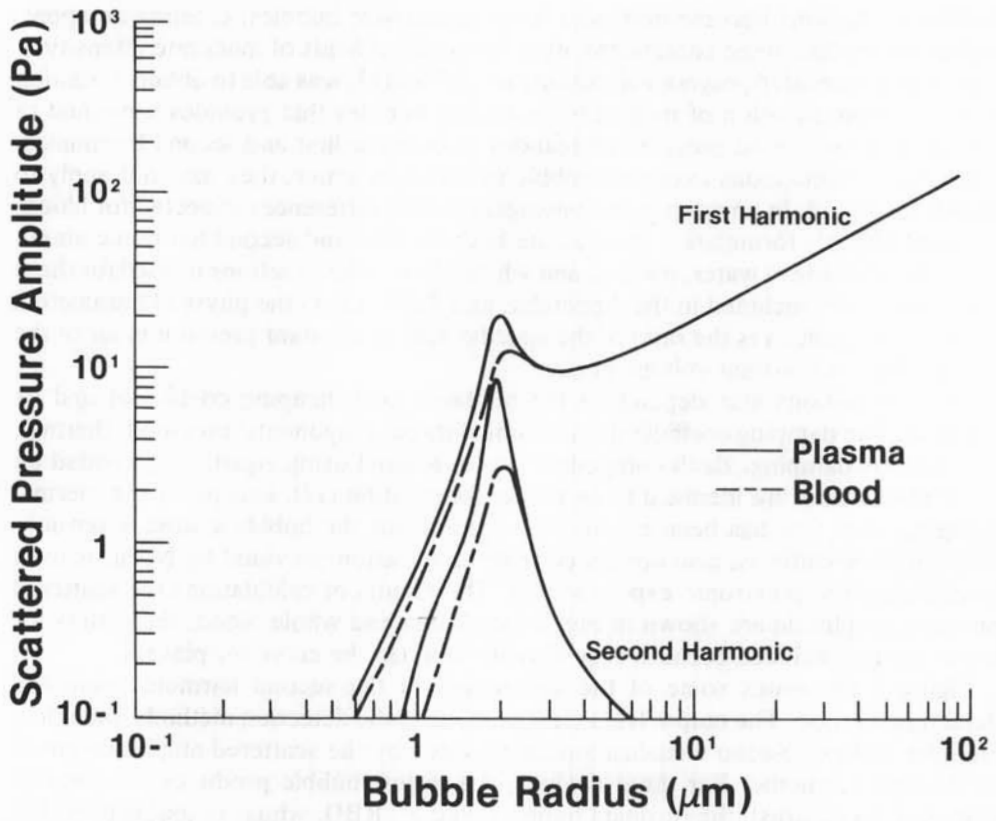

Fig. 1. Theoretical scattered pressure amplitudes of first and second harmonics for various bubble sizes (fundamental frequency 1.62 MHz; detector 6 mm from bubble).

contrast to Doppler output, the RBD does not depend on a frequency shift and will therefore respond to stationary bubbles.

METHODS

Figure 2 shows a cross-sectional view of the detector, which has been described in detail elsewhere (13). Briefly, it consists of a cylinder (15 mm in diameter and 20 mm long) made from sound-absorbing rubber (SOAB) that is split in half and has a 4-mm hole in the center to accommodate either a Tygon® tube or a small blood vessel. Two piezoelectric transducers are mounted at right angles to each other. The transmitting transducer of the detector is 4.8 mm in diameter and has a resonance frequency of 1.62 MHz. The receiving transducer is 3.2 mm in diameter and has a resonance frequency of 3.24 MHz. The transducers were positioned above the blood vessel for all venous measurements. Because of inflexible cables, which were used in this prototype, this position proved impractical for arterial measurements, thus the transducers were positioned below the blood vessel to obtain these measurements. Degassed aquasonic gel was squirted liberally into the interior of the detector before it was secured around the blood vessel by using a Dacron® ribbon.

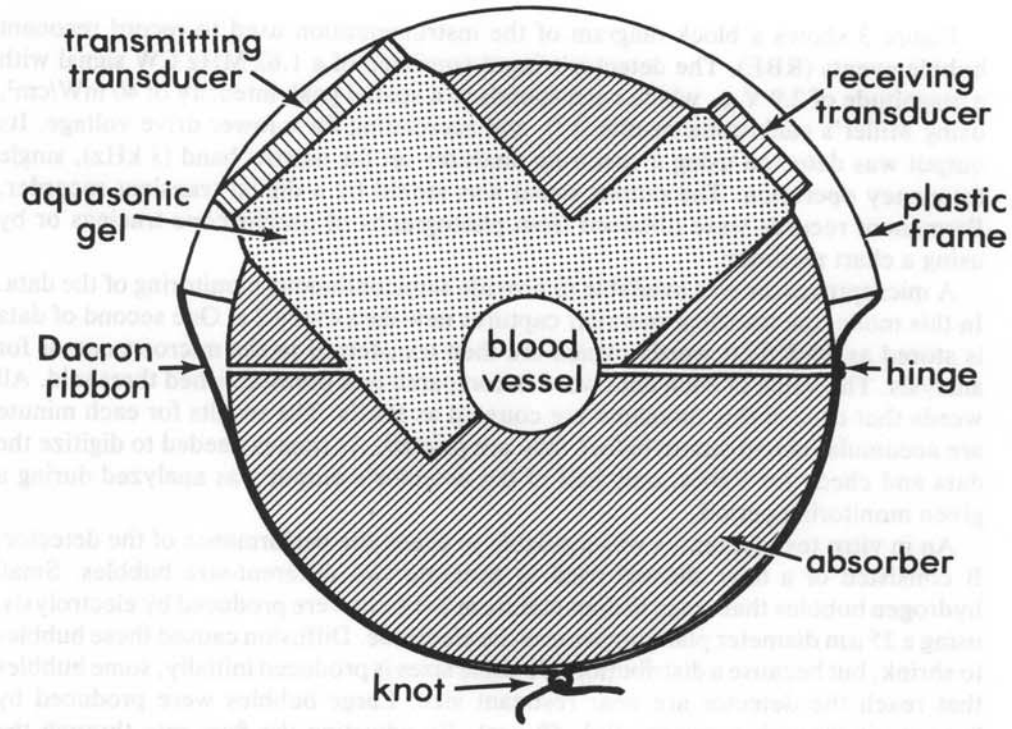

Fig. 2. Cross-sectional view of resonant bubble detector. Transmitting transducer has a resonant frequency of 1.62 MHz whereas the receiving transducer has a resonant frequency of 3.24 MHz.

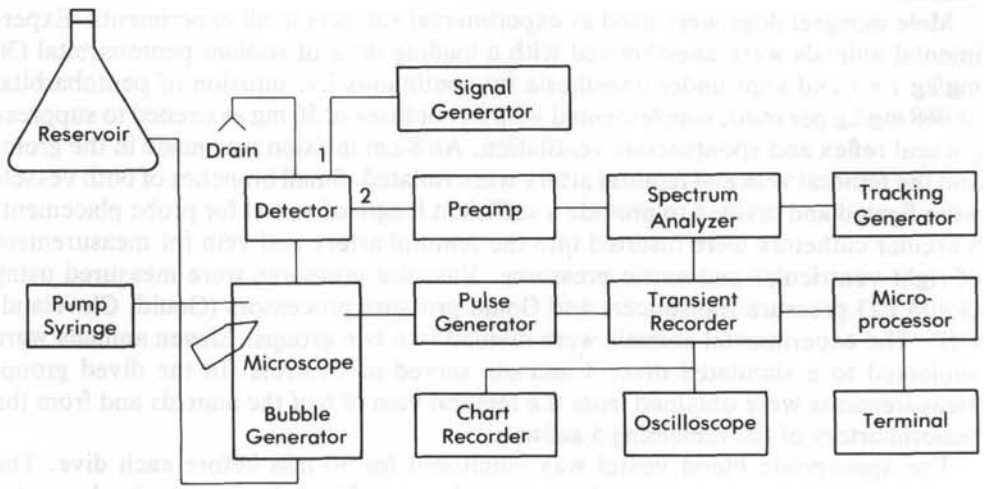

Fig. 3. Block diagram of equipment used to record resonant bubble events. Bubble generator produced 500 μm diameter bubbles by forcing air through a syringe and small hydrogen bubbles (2–14 μm in diameter) by electrolysis. A 1.62 MHz CW input signal was applied to channel 1 of the detector. The second harmonic signal (3.24 MHz) was detected at channel 2 using a spectrum analyzer and tracking generator set to operate as a narrow band-pass filter.

Figure 3 shows a block diagram of the instrumentation used to record resonant bubble events (RBE). The detector's input consisted of a 1.62 MHz CW signal with a magnitude of 2.9 V_{rms}, which corresponds to a spatial peak intensity of 40 mW/cm^2, using Miller's calibration results (13), and accounting for a lower drive voltage. Its output was detected using a spectrum analyzer set for narrow band (3 kHz), single frequency operation. The output signal was stored by a digital transient recorder. Permanent records were obtained from photographs of oscilloscope tracings or by using a chart recorder.

A microprocessor was available to provide semicontinuous monitoring of the data. In this mode, the transient recorder captures new data every 2 s. One second of data is stored as 2048 8-bit words, which are then transferred to the microprocessor for analysis. The value of each data word is compared to a preestablished threshold. All words that exceed this threshold are counted as RBEs. The results for each minute are accumulated and stored before they are printed. As time is needed to digitize the data and check for RBEs, only half of the detector's output was analyzed during a given monitoring period.

An in vitro test apparatus was available to check the performance of the detector. It consisted of a flow channel used to generate two different-size bubbles. Small hydrogen bubbles that range in diameter from 2–14 μm were produced by electrolysis, using a 25 μm diameter platinum wire as the electrode. Diffusion caused these bubbles to shrink, but because a distribution of bubble sizes is produced initially, some bubbles that reach the detector are near resonant size. Large bubbles were produced by forcing air through a syringe (i.d. 50 μm). By adjusting the flow rate through the channel and the pressure applied to the syringe, a steady stream of 500 μm diameter bubbles was produced. A surfactant (liquid Ivory soap, 1 drop/l) and an electrolyte (sodium sulfate, 1 g/l) were added to the distilled water reservoir that fed the flow channel.

Male mongrel dogs were used as experimental subjects in all experiments. Experimental animals were anesthetized with a loading dose of sodium pentobarbital (30 mg/kg i.v.) and kept under anesthesia by continuous i.v. infusion of pentobarbital (0.068 mg/kg per min), supplemented with i.v. boluses of 50 mg as needed to suppress corneal reflex and spontaneous ventilation. An 8-cm incision was made in the groin, and the femoral vein and femoral artery were isolated. Small branches of both vessels were ligated and divided to provide a sufficient length of vessel for probe placement. Vascular catheters were inserted into the femoral artery and vein for measurement of right ventricular and aortic pressures. Vascular pressures were measured using Gould P23 pressure transducers and Gould pressure processors (Gould, Cleveland, OH). The experimental animals were divided into two groups. Eleven animals were subjected to a simulated dive; 4 animals served as controls. In the dived group, measurements were obtained from the femoral vein of 6 of the animals and from the femoral artery of the remaining 5 animals.

The appropriate blood vessel was monitored for 30 min before each dive. The detector was then removed and the animal was subjected to pressurized air at a controlled rate of descent (100 ft/min). After reaching an equivalent pressure of 300 fsw, the pressure was held constant for 14 min, yielding a total bottom time of 17 min. The subject was then decompressed at a controlled rate of ascent (60 ft/min) and monitored until acute symptoms of decompression sickness occurred. For this experiment, a doubling in right ventricular systolic pressure within 10 min of surfacing

constituted severe decompression sickness. If this degree of elevation did not occur, the dog was subjected to one or more repeat dives to 300 fsw, each with a total bottom time of 8 min, until the desired ventricular pressure elevation occurred within the 10-min postdive observation period. After decompression sickness was confirmed, the animal's femoral blood vessel was monitored for an additional 3 h or until the animal's death. At the end of the experiment animals were killed by intravenous injection of KC1, and an autopsy was performed.

The control animals were treated in a fashion identical to the dived animals, except they were not exposed to raised environmental pressure. Before each sham dive, the dog was monitored for 45 min; the first 30 min the animal was monitored for arterial flow and the last 15 min for venous flow. After the dive, the dog was monitored for a total of 180 min; the first 150 min the dog's venous flow was monitored, and the last 30 min the arterial flow was monitored.

RESULTS

Figure 4 represents the response of the detector to a variety of different cases. Its in vitro response to small bubbles generated at a time equal to zero is shown in Fig. 4*a*. For this case, the bubbles took approximately 100 ms to pass through the flow channel before they reached the detector. For comparison, the detector's in vitro response to large bubbles is shown in Fig. 4*b*. This plot represents only a slight increase over the baseline normally observed when no bubbles are produced.

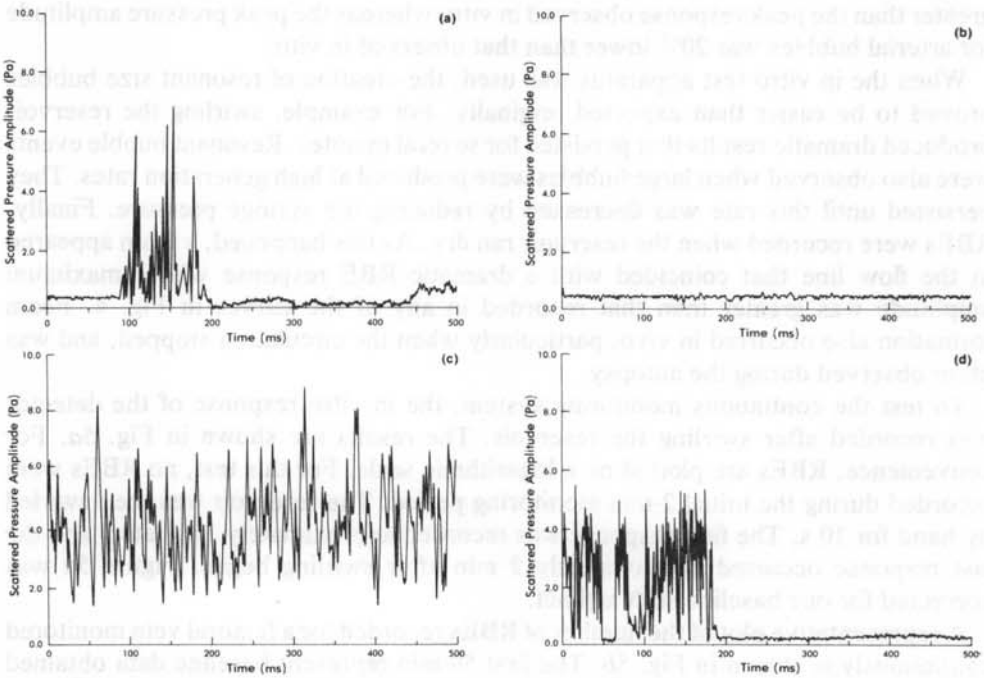

Fig. 4. In vitro response of the resonant bubble detector to *(a)* bubbles near resonant size (4 μm diameter), and *(b)* to 500 μm diameter bubbles. In vivo response of resonant bubble detector recorded on *(c)* the femoral vein, and *(d)* the femoral artery of dogs subjected to rapid decompression.

The detector's in vivo response recorded at the femoral vein of a dog subjected to a single dive after the usual dive protocol is shown in Fig. 4*c*. This response was recorded 8 min after surfacing. The response of control animals was virtually identical to that shown in Fig. 4*b*. Bubble responses for arterial flow were generally more difficult to observe. In an effort to enhance their detection, an experimental animal was subjected to a series of repeat dives. Bubbles were observed visually in the femoral vein of this dog after the second dive, although no RBEs were recorded in the artery during a 13-min monitoring period. The dog was subjected to a third dive, and this time a response in the femoral artery was recorded 9 min after surfacing (Fig. 4*d*).

From Fig. 4*a* and *b*, the gain in the detector's output for small bubbles as compared to its output for large bubbles was 32 dB, approximately the same as the gain reported by Miller (13). These figures illustrate one of the detector's unique features, its ability to discriminate between different-size bubbles.

In Fig. 4, the magnitude of each response curve is based on calibration results reported by Miller (13) but corrected for a lower incident intensity used in this study. The calibration was estimated from sensitivity measurements of both the transmitting and receiving transducers, an estimate of the attenuation of the acoustic field due to the Tygon® tube based on hydrophone measurements (Miller used an attenuation factor of 1.6 at the first harmonic and 2.0 at the second harmonic), and an estimate of the spatial average intensity within the Tygon® tube. Because of these approximations, the scattered pressure amplitude should be considered only an order-of-magnitude estimate. The peak pressure amplitude for the venous response was 30% greater than the peak response observed in vitro whereas the peak pressure amplitude for arterial bubbles was 20% lower than that observed in vitro.

When the in vitro test apparatus was used, the creation of resonant size bubbles proved to be easier than expected originally. For example, swirling the reservoir produced dramatic results that persisted for several minutes. Resonant bubble events were also observed when large bubbles were produced at high generation rates. They persisted until this rate was decreased by reducing the syringe pressure. Finally, RBEs were recorded when the reservoir ran dry. As this happened, a foam appeared in the flow line that coincided with a dramatic RBE response whose maximum amplitude was greater than that recorded in any of the curves in Fig. 4. Foam formation also occurred in vivo, particularly when the circulation stopped, and was often observed during the autopsy.

To test the continuous monitoring system, the in vitro response of the detector was recorded after swirling the reservoir. The results are shown in Fig. 5*a*. For convenience, RBEs are plotted on a logarithmic scale. For this test, no RBEs were recorded during the initial 2-min monitoring period. The reservoir was then swirled by hand for 10 s. The first response was recorded approximately 10 s later, and the last response occurred approximately 2 min after swirling began. Figure 5*a* was corrected for one baseline shift artifact.

A representative plot of the number of RBEs recorded for a femoral vein monitored continuously is shown in Fig. 5*b*. The first 50 min represent baseline data obtained before the dive whereas data after 50 min correspond to monitoring started 15 min after surfacing. The interval between 50 and 100 min represents a saturation period during which an RBE was detected in virtually every data sample captured by the

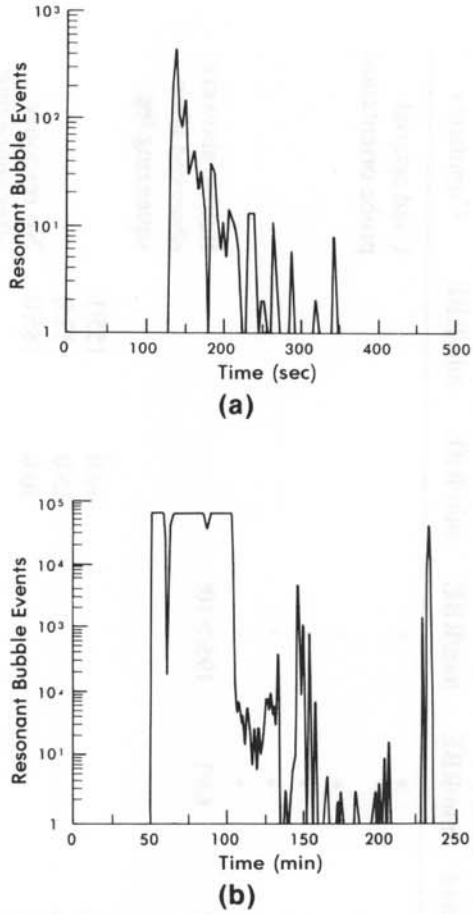

Fig. 5. Continuous monitoring results recording *(a)* the in vitro response of the resonant bubble detector after swirling the reservoir, and *(b)* its in vivo response for the femoral vein of a dog subjected to rapid decompression.

transient recorder. During this period a foam was observed flowing at the top of the vessel.

All results obtained for the 15 dogs monitored in this study are summarized in Table 2. This table is separated into three groups differentiating the blood vessel monitored: 6 dived dogs were subjected to venous monitoring, 5 dived dogs to arterial monitoring, and 4 dogs were controls. The table lists each dog's weight, total number of dives, and whether or not the dog died before the planned monitoring was completed. Comments document deviations from standard protocol that include inadvertent use of the wrong probe orientation or the wrong RBE threshold. The overall response for each dog was highly variable, even within a particular group. Continuous monitoring results are summarized in Table 2 in terms of the monitoring interval in minutes and the total number of RBEs recorded. For the data shown in Fig. 5*b*, the dog's vein was monitored for a total of 195 min after the dive, during which time more than 10^6 RBEs were detected.

TABLE 2

RESULTS OF RESONANT BUBBLE MONITORING WITHIN FEMORAL BLOOD VESSELS OF DOGS SUBJECTED TO RAPID DECOMPRESSION

Dog	Weight, kg	Vessel Monitored	Early Death	Total Number of Dives	Resonant Bubbles Detected	Venous Response		Arterial Response		Comments
						Before Dive, min/RBE	After Dive, min/RBE	Before Dive, min/RBE	After Dive, min/RBE	
1	13.6	Vein	N	2	Y	*	*			Used arterial probe orientation
2	20.0	Vein	N	2	Y	*	*			
3	16.3	Vein	N	3	Y	*	*			
4	16.3	Vein	Y	1	Y	*	*			
5	13.2	Vein	Y	2	Y	*	*			
6	15.0	Vein	N	1	Y	65/1	195/>10^6			Bubble showers observed after squeezing leg
1	13.6	Artery	N	1	N			40/0	155/1	
2	15.0	Artery	Y	1	N			15/0	17/0	
3	16.8	Artery	N	3	N			30/0	185/0	No response after squeezing leg
4	15.0	Artery	Y	2	Y			30/0	—	Dog died; no data recorded after dive
5	15.4	Artery	N	3	Y			35/0	155/1	

TABLE 2 (continued)
RESULTS OF RESONANT BUBBLE MONITORING WITHIN FEMORAL BLOOD VESSELS OF DOGS SUBJECTED TO RAPID DECOMPRESSION

Dog	Weight, kg	Vessel Monitored	Early Death	Total Number of Dives	Resonant Bubbles Detected	Venous Response		Arterial Response		Comments
						Before Dive, min/RBE	After Dive, min/RBE	Before Dive, min/RBE	After Dive, min/RBE	
1	22.3	Vein/Artery	N	Sham	N	15/0	160/12	—	35/11	Venous threshold used for arterial observations
2	8.8	Vein/Artery	N	Sham	N	25/0	40/0	—	30/3	Venous monitoring period after dive reduced
3	22.7	Vein/Artery	N	Sham	N	20/0	150/6	30/0	30/4	
4	14.7	Vein/Artery	N	Sham	N	15/0	140/1	35/0	40/0	

*Continuous monitoring system was developed after these experiments were completed.

Some difficulty was encountered in obtaining reliable RBE data. There were many falsely positive data that may have registered as a result of electrical noise or poor coupling to the blood vessel, in part due to movement of the probe during respiration and decreases in blood pressure as the dog died. Often baseline shifts and electrical noise were distinguished from RBEs because of distinct differences in their temporal and spectral components. The results reported in Table 2 represent data corrected for distinguishable artifacts; thus some monitoring periods are missing or reduced from what is specified in the protocol.

During venous monitoring, resonant bubbles were detected in all 6 dogs, although in some cases a dramatic response was observed only when the leg was squeezed by hand. During arterial monitoring, 3 of 5 dogs in the group showed no resonant bubbles, even when the hindlimb was squeezed. One dog showed resonant bubbles in the artery but this dog died during the monitoring period. The other dog showed a weak response (short duration and low frequency of occurrence) in the artery after being subjected to a total of 3 dives. No resonant bubbles were detected in the control animals, although occasional artifacts, probably due to electrical noise, were observed.

A separate experiment was conducted to test the likelihood of detecting an artifact. No dog was used in this experiment. The probe was placed around a piece of Tygon® tube filled with aqua-gel and then taped to the specimen table of the compression chamber. An effort was made to duplicate all conditions that occur during a typical experiment in this study. The probe was monitored for a total of 10 h on 2 separate days. During that time, one RBE was detected.

DISCUSSION

Past calculation of the scattered pressure amplitudes of the first and second harmonics for water, blood plasma, and whole blood has shown that the same basic response curve is expected for each fluid (Fig. 1). The main difference occurs with whole blood, whose resonant peak is attenuated compared to the values for plasma and water, which are nearly identical. On the basis of this finding, we expected greatly attenuated signals from the femoral vessels when compared to the in vitro Tygon® tube system. We observed the response from the femoral vessels, however, to be greater than that from the in vitro system. These results suggest that either the Tygon® tubing attenuated greatly the second harmonic signal or that the scattered pressure amplitude curve for plasma rather than blood best describes the in vivo experimental system. Based on estimates of impedance and the absorption coefficient, we believe the differences in attenuation between Tygon® tubing and blood vessels are small. Therefore, we believe that our observation supports Nishi's (14) suggestion that it is probably inappropriate to use the properties of whole blood to calculate acoustic effects on microbubbles smaller than a red blood cell.

This investigation offers no real insight into the origin, evolution, or eventual decay of the 4 μm diameter microbubbles that have been detected. In fact, their existence in vivo in the quantities observed is surprising because surface tension for a bubble this small creates a high internal pressure that tends to dissolve the bubble within a few milliseconds. Additional research is needed to study this phenomenon. Until new results are available, though, we can only speculate about the origin and evolution of these microbubbles.

Perhaps in vivo microbubbles are stabilized by an organic skin, as Johnson and Cooke (19) suggested regarding bubbles in seawater and Yount (20) suggested in the decompression context. They may also be formed by fission. Evidence to support this latter hypothesis comes from the results of large bubbles in vitro, which may be explained as follows: As the rate of generation of large bubbles increases, their size and separation distance decreases. When the bubbles are less than 300 μm in diameter, a collision may result in bubble fission and not coalescence (21, 22). Although the fission products may be larger than resonant size, they may dissolve partially to resonant size before reaching the detector, producing the observed resonant bubble events.

Microbubbles apparently also form as part of the distribution of bubble sizes that comprise a foam and they may be stabilized partially by the foam. Using a thermodynamic analysis of the stability of bubbles in a closed volume, Ward et al. (23) predicted that for large concentrations of bubbles a stable equilibrium state exists for micron-sized bubbles. The in vitro formation of a foam as the reservoir ran dry in this study produced a dramatic response, with a peak amplitude higher than any response observed in vivo. At least two explanations may account for this result. First, the foam allows more microbubbles to exist within the probe's detection volume, and second, the foam constrains some microbubbles to be closer to the detector.

The data summarized in Table 2 show that microbubbles are detected more readily in venous flow than in arterial flow. All 6 dogs monitored for venous flow produced positive evidence of resonant bubbles. In contrast, the first 3 dogs monitored for arterial flow showed no evidence of resonant bubbles. Although the 4th dog showed a positive response, this dog was seriously ill and died early. The 5th dog was the only one to survive the entire monitoring period and show evidence of resonant bubbles in the arterial flow. The response recorded was weak and of short duration, even though this dog was subjected to the most severe decompression stress used in the study. The difference in peak amplitude between the arterial response and the venous response is most likely due to the difference in probe orientation and to increased attenuation through the arterial vessel wall.

These results indicate that microbubbles 4 μm in diameter are detected readily in the venous flow of dogs suffering from decompression sickness, but are much less likely to occur in the arterial flow. A number of hypotheses are offered to explain this result. Microbubbles may form de novo in both venous and arterial circulation. The rate of formation in the arterial system may be less because of increased ambient pressure and differences in gas concentrations.

In addition, microbubbles may form in tissues and enter the circulatory system through ruptures in the capillary network. Then they may flow unimpeded through the venous system but may dissolve before reaching the lungs. Some microbubbles may reach the lungs but be filtered by the pulmonary capillary bed because they have coalesced into larger bubbles or because they adhere to the endothelial lining of the pulmonary vascular bed. Data collected by Butler and Hills (24) suggest that if a cutoff diameter exists for filtration by pulmonary circulation in dogs under normal conditions, it must be less than 22 μm. Finally, the microbubbles may pass through the lungs but dissolve before reaching the femoral artery. Although our results demonstrate clearly a higher frequency of 4 μm diameter bubbles in femoral venous

blood than in femoral arterial blood during decompression sickness, they do not allow us to select one of these hypotheses in favor of another.

Interpreting resonant bubble event data is difficult, as illustrated by the following idealized example. Assume only one resonant bubble is present within the detection volume at a given time and a response is independent of bubble location within that volume. For this example, the detection volume is given by the inner diameter of the blood vessel and the area of the receiving transducer. Also assume that the blood velocity is uniform and resonant bubbles pass unimpeded through the detector. Using mean velocities of 15 cm $\cdot$ s^{-1} (25) for the femoral vein and 50 cm $\cdot$ s^{-1} (26) for the femoral artery, a resonant bubble remains within the detection zone for 21 ms during venous monitoring and 6 ms during arterial monitoring. Because the transient recorder samples the detector's output every 0.5 ms, dividing the number of RBEs by 42 or 12 for venous and arterial measurements, respectively, determines the number of resonant bubbles. In reference to Fig. 5*b*, 2800 resonant bubbles/min were detected during the first 50 min of monitoring after surfacing (a factor of 2 is needed to account for RBEs missed while processing data).

Because this method cannot distinguish multiple resonant bubbles within the detection zone, it detects only the minimum number of resonant bubbles present, assuming the bubbles pass unimpeded through the detector. A similar defect applies for imaging devices that respond to the maximum possible diameter of a bubble and produce the same response for a cluster of smaller bubbles (7).

Although the assumption that a response is independent of bubble location also seems to be a major defect in the model described in the above example, this assumption may not be as restrictive as it first appears. By using a suitable detection threshold, spatial variations in the incident field and differences due to distance from the receiver can be eliminated.

Another factor that complicates the interpretation of RBE data is the effect of radiation force produced by the incident acoustic field. Miller estimates that a resonant bubble would be accelerated by radiation force and would reach a terminal velocity of approximately 10 cm $\cdot$ s^{-1} within 1.0 ms after entering the detection volume (13). Although this may not be a problem for arterial measurements where the higher mean blood velocity dominates, corrections may be needed to account for changes in bubble trajectory during venous measurements.

An improved detector design may facilitate interpretation of the data. For example, pulse conditions could be used to minimize the effects of radiation force. Range gating and focusing could be used to sharpen the detection volume, which would enhance the possibility of detecting multiple resonant bubbles and would reduce variations due to differences in bubble location. Finally, a direct measurement of the velocity profile, perhaps using a Doppler technique, would aid in computing the number of resonant bubbles.

The data presented suggest that in vivo RBD is feasible using the second harmonic emission technique, and we would recommend its use in studies of the origin and generation of early decompression sickness. This technique may prove useful in other fields as well. Figure 4*a* and *b* illustrate one of the unique features of this method, namely, its ability to detect only bubbles near resonant size. The development of this probe is a significant step toward the final production of a device that measures the entire distribution of bubble sizes. Our early stage of development prototype was used to detect 4 μm diameter bubbles in both the femoral artery and the femoral vein

of dogs suffering from decompression sickness. Resonant bubbles were detected more readily in the femoral vein, which suggests the possibility that the lungs effectively filter bubbles from the arterial flow. Although instrumentation was developed to continuously monitor the experimental animals for resonant bubble events, interpretation of these results is difficult and can not be used directly to determine the number of resonant bubbles. Modifications are possible to enhance the quantification of these data, however.

The authors wish to express their gratitude to Mr. David Legrys for photographic assistance, and to J. T. Johnson, J. Harrington, and Mrs. Linda Thomas for technical assistance with the experiments. The authors are also grateful to Mrs. Maureen Darmody for her excellent editorial assistance.

This study was supported by the Naval Medical Research and Development Command, Research Task No. M0099.PN001.1170. The opinions and assertions contained herein are the private ones of the authors and are not to be construed as official or reflecting the views of the Navy Department or the naval service at large.

The experiments supported herein were conducted according to the principles set forth in the "Guide for the Care and Use of Laboratory Animals," Institute of Laboratory Animal Resources, National Research Council, DHHS, Pub. No. (NIH) 78-23.—*Manuscript received for publication August 1984; revision received April 1985.*

Christman CL, Catron PW, Flynn ET, Weathersby PK. Détection de microbulles in vivo durant la maladie de décompression à l'aide d'un détecteur de bulle à résonnance d'harmonique secondaire. Undersea Biomed Res 1986; 13(1):1–18.—Une méthode de résonnance pour la détection de bulle, basée sur la technique de l'harmonique secondaire, à été utilisée pour la surveillance du système vasculaire fémoral chez des chiens soumis à des décompressions rapides. Pour cette étude, le détecteur consistait de deux tranducteurs acoustiques montés à angle droit, l'un par rapport à l'autre, et préemballés dans une sorte de manchon périvasculaire. Ce détecteur répond sélectivement aux bulles près de la grosseur de résonnance seulement (4.2 μm de diamètre); les particules solides et les grosses bulles ne produisent pas de réponse. Le détecteur fut utilisé pour surveiller un total de 15 chiens. Onze chiens furent soumis à une série de plongées sousmarines simulées jusqu'à l'apparition de symptômes aigus de maladie de décompression; 4 chiens servirent de témoins. Chez le groupe de plongée, soit la veine fémorale ou l'artère fémorale fut surveillée. Des bulles résonnantes furent observées dans les veines fémorales des 6 chiens surveillés à cet endroit. Pendant la surveillance artérielle, la majorité des chiens ne fournirent aucune réponse, mais une faible réponse occasionnelle fut détectée chez 2 de ces chiens. Aucune bulle résonnante ne fut détectée dans l'artère ou la veine fémorale des animaux témoins. Les données suggèrent que cette méthode de détection de bulle est possible pour l'utilisation in vivo. De plus, les bulles de 4 μm de diamètre sont beaucoup plus prédominantes dans les veines des chiens souffrant de la maladie de décompression qu'elles le sont dans les artères de ces animaux, présumément parce qu'elles sont filtrées efficacement par la circulation pulmonaire. Les modifications de cette méthode sont discutées pour augmenter sa précision et son application pour quantifier la grosseur des bulles, ainsi que leur location et leur nombre.

détection de microbulle
détection ultrasonique de bulle
probe implantée
maladie de décompression
non linéaire
résonnance
harmonique secondaire

REFERENCES

1. Maroon JC, Albin MS. Air embolism diagnosed by Doppler ultrasound. Anesth Analg 1974; 53:399–402.
2. Lubbers J, Van den Berg JW. An ultrasonic detector for microgasemboli in a bloodflow line. Ultrasound Med Biol 1976; 2:301–310.
3. Evans A. Ultrasonic surveillance of decompression. In: Bennett PB, Elliott DH, eds. The physiology and medicine of diving and compressed air work. London: Bailliere Tindall, 1975: 417–434.

4. Smith KH, Spencer MP. Doppler indices of decompression sickness: their evaluation and use. Aerosp Med 1970; 41:1396–1400.
5. Nishi RY. Ultrasonic detection of bubbles with Doppler flow transducers. Ultrasonics 1972; 10(4):173–179.
6. Nishi RY, Livingstone SD. Intravascular changes associated with hyperbaric decompression: theoretical considerations using ultrasound. Aerosp Med 1973; 44:179–183.
7. Rubissow GJ, MacKay RS. Decompression study and control using ultrasonics. Aerosp Med 1974; 45:473–478.
8. Daniels S, Davies JM, Paton WDM, Smith EB. The detection of gas bubbles in guinea pigs after decompression from air saturation dives using ultrasonic imaging. J Physiol 1980; 308:369–383.
9. Beck TW, Daniels S, Paton WDM, Smith EB. Detection of bubbles in decompression sickness. Nature 1978; 276:173–174.
10. Welsby VG, Safar MH. Acoustic nonlinearity due to microbubbles in water. Acustica 1969–70; 22:177–182.
11. Medwin H. Counting bubbles acoustically: a review. Ultrasonics 1977; 15(1):7–13.
12. Horton JW, Wells CH. Resonance ultrasonic measurements of microscopic gas bubbles. Aviat Space Environ Med 1976; 47:777–781.
13. Miller DL. Ultrasonic detection of resonant cavitation bubbles in a flow tube by their second-harmonic emissions. Ultrasonics 1981; 19(5):217–224.
14. Nishi RY. The scattering and absorption of sound waves by a gas bubble in a viscous liquid. Acustica 1975; 33(2):65–74.
15. Altman PL, Dittmer DS, eds. Respiration and circulation. Bethesda: Federation of American Societies for Experimental Biology, 1971:26.
16. Lewin S. Blood serum surface tension and its potential. Br J Haematol 1972; 22:561–566.
17. Devin C Jr. Survey of thermal, radiation, and viscous damping of pulsating air bubbles in water. J Acoust Soc Am 1959; 31:1654–1667.
18. Crum LA. The polytropic exponent of gas contained within air bubbles pulsating in a liquid. J Acoust Soc Am 1983; 73:116–120.
19. Johnson BD, Cooke RC. Generation of stabilized microbubbles in seawater. Science 1981; 213:209–211.
20. Yount DE. Skins of varying permeability: a stabilization mechanism for gas cavitation nuclei. J Acoust Soc Am 1979; 65:1429–1439.
21. Hills BA. Air embolism: fission of microbubbles upon collision in plasma. Clin Sci Mol Med 1974; 46:629–634.
22. Yount DE. A model for microbubble fission in surfactant solutions. J Colloid Interface Sci 1983; 91:349–360.
23. Ward CA, Tikuisis P, Venter RD. Stability of bubbles in a closed volume of liquid-gas solution. J Appl Physiol 1982; 53:6076–6084.
24. Butler BD, Hills BA. The lung as a filter for microbubbles. J Appl Physiol 1979; 47:537–543.
25. Kountz SL, Dempster WJ, Shillingford JP. Application of a constant indicator dilution method to the measurement of local venous flow. Circ Res 1964; 14:377–386.
26. Histand MB, Miller CW, McLeod FD Jr. Transcutaneous measurement of blood velocity profiles and flow. Cardiovasc Res 1973; 7:703–712.

APPENDIX

The first harmonic scattered pressure amplitude, p_{s1}, is given by:

$$p_{s1} = p_1 \Omega^2 X_1 R_0 / r$$

where p_1 is the incident acoustic pressure amplitude, R_0 is the initial radius of the bubble before ultrasound is applied, and r is the distance from the center of the bubble (13). The normalized frequency Ω equals ω/ω_0, where ω is the acoustic driving frequency. The linear resonance frequency of the bubble, ω_0, is given by:

$$\rho\omega_0^2 R_0^2 = 3\kappa\left(p_0 + \frac{2\sigma}{R_0}\right) - \frac{2\sigma}{R_0}$$

where ρ is the density of the liquid, κ is the polytropic exponent, p_0 is the ambient static pressure, and σ is the surface tension. The factor X_1 can be expressed as:

$$X_1 = \left[(1-\Omega^2)^2 + \Omega^2\delta^2\right]^{-1/2}$$

where δ is the total damping coefficient.

The second harmonic scattered pressure amplitude, p_{s2}, is given by:

$$p_{s2} = \left(\frac{p_1^2}{\rho\omega_0^2 R_0^2}\right) \Omega^2 X_1^2 Y X_2 R_0/r$$

where

$$Y = \left\{\left[\frac{5\Omega^2}{2} + \frac{3\kappa(p_0+2\sigma/R_0)(3\kappa+1)-4\sigma/R_0}{2\rho\omega_0^2 R_0^2}\right]^2 + \Omega^2\delta^2\right\}^{1/2}$$

and

$$X_2 = \left[(1 - 4\Omega^2)^2 + 4\Omega^2\delta^2\right]^{-1/2}$$

The total damping coefficient, δ, equals the sum of three factors: δ_r, δ_{th}, and δ_v (14). The radiation damping coefficient, δ_r, is given by:

$$\delta_r = \omega R_0/c_w$$

where c_w is the acoustic velocity within the liquid. The thermal damping coefficient δ_{th} can be written as:

$$\delta_{th} = \frac{\omega_0^2\delta_t}{\omega^2 g}\left(1 + \frac{2\sigma}{R_0 p_0}\right)$$

where δ_t is called the thermal damping constant. The factor g is given by:

$$g = 1 + \frac{2\sigma}{R_0 p_0}\left(1 - \frac{\epsilon}{3\gamma}\right)$$

where ϵ is called the stiffness of the bubble and γ is the ratio of the specific heats at constant pressure and at constant volume in air. The thermal damping constant is given by:

$$\delta_t = \frac{\dfrac{\sinh d + \sin d}{\cosh d - \cos d} - \dfrac{2}{d}}{\dfrac{\sinh d - \sin d}{\cosh d - \cos d} + \dfrac{d}{3(\gamma - 1)}}$$

where

$$d = R_0\left(\frac{2\gamma\omega}{D}\right)^{1/2}$$

D is the thermal diffusivity of the liquid. The stiffness of the bubble can be expressed as:

$$\epsilon = (1 + \delta_r^2)\left[\frac{3(\gamma - 1)}{d}\frac{\sinh d - \sin d}{\cosh d - \cos d} + 1\right]$$

The polytropic exponent, κ, equals γ/ϵ. Finally, the viscous damping coefficient, δ_v, is given by:

$$\delta_v = \frac{4\eta}{\omega\rho R_0^2}$$

where η is the viscosity of the liquid.